ORIGINAL RESEARCH ARTICLE

Analytical Study on Reliability Improvement and Rationalization of Maintenance of High-Strength Steel by Surface Crack Nondamaging Technology (in Case of Stress Ratio $R = -1.0$)

Kyoung-Hee Gu ⓘ, Kotoji Ando, and Ki-Woo Nam ⓘ

The threshold stress intensity factor (ΔK_{th}) has dependent on the crack size during the propagation of microfatigue cracks. Ando et al. proposed a new surface crack nondamaging technology to evaluate this dependence. This technology has been validated in situations where the stress ratio is positive $(R > 0)$. However, to expand the application range of this technology, it is necessary to verify its applicability in the case of stress ratio $R < 0$. Therefore, this applicability was examined based on the results of the previous experiments. This study aims to investigate the effect of the residual stress distribution (RS1) of cavitation peening (CP) in the case of $R < 0$ on the harmless crack size (a_{hml}) of steel with crack-like surface defects. To compare with the residual stress distribution (RS1) of CP, two types (RS2 and RS3) with different residual stress distributions were used. The surface residual stresses of RS1, RS2, and RS3 were the same, but the distribution of depth from the surface was different. Compressive residual stress is the dominant factor that renders surface defects harmless. The depth of the residual stress significantly influenced a_{hml}. Moreover, the trend of the defect size that can be rendered harmless, estimated based on fracture mechanics, was slightly larger than that of the experimental results. However, surface crack nondamaging technology can be applied even when the stress ratio is negative $(R < 0)$.

1. Introduction

The fatigue limit of metals is determined by many slip bands, and many intrusions and extrusions are formed because of their active activity (Ref 1). Therefore, Ando et al.(Ref 2) used the fatigue limit as the stress that defines the nonlinear region of the crack tip and proposed Eq 1 for the threshold stress intensity factor (ΔK_{th}) with crack size dependence. In the case of the stress ratio $R = 0$ examined in research by Nakagawa et al.(Ref 3), the following three items were clarified using Eq 1 to obtain the fatigue fracture behavior of the peening material with a pre-crack. ① The harmless crack depth (a_{hml}) of the peening material with a pre-crack and the fatigue limit of the pre-crack material that cannot be rendered harmless can be predicted with high accuracy using Eq 1. Nondamaging surface

Kyoung-Hee Gu, Department of Marine Convergence Design Engineering, Pukyong National University, 45 Yongsoro, Namgu, Busan 48513, Korea; **Kotoji Ando**, Faculty of Engineering, Yokohama National University, 79-5 Tokiwadai Hodogaya, Yokohama 240-8501, Japan; and and **Ki-Woo Nam**, Department of Materials Science and Engineering, Pukyong National University, 45 Yongsoro, Namgu, Busan 48513, Korea. Contact e-mail: namkw@pknu.ac.kr.

List of Symbols	
σ_O	Residual stress of outmost surface
σ_{max}	Maximum stress
σ_{min}	Minimum stress
$\Delta\sigma$	Stress range
Δ_w	Fatigue limit of nonpeened smooth specimen
Δ_{wp}	Fatigue limit of peened smooth specimen
Δ_{wc}	Fatigue limit of nonpeened crack specimen
Δ_{wcp}	Fatigue limit of peened crack specimen
ΔK_{th}	Threshold stress intensity factor
ΔK_{th}^R	Threshold stress intensity factor for a certain stress ratio
$\Delta K_{th(l)}^R$	Threshold stress intensity factor range for large cracks
ΔK_{Tr}	Effective stress intensity factor range
$\Delta K_{Tr(A)}$	Effective stress intensity factor range at the deepest crack (point A)
$\Delta K_{Tr(C)}$	Effective stress intensity factor range at surface crack (point C)
ΔK_{ap}	Stress intensity factor range under applied stress
K_r	Stress intensity factor due to the compressive residual stress
As	Aspect ratio
$Non\text{-}CP$	Non-cavitation peened specimen
CP	Cavitation peened specimen
a	Crack depth of semi-elliptical crack in finite plate
a_{cr}	Critical crack depth that considers the safety factor
a_{hml}	Maximum harmless crack depth
a_{NDI}	Minimum detectable crack depth via nondestructive inspection
$2c$	Crack length of semi-elliptical crack

d_0	Depth at which the compressive residual stress is 0
$2l$	Through crack length in infinite plate
l_e	Equivalent half-crack length
R	Stress ratio
RS1	Residual stress by cavitation peening
RS2	Residual stress by double-shot peening
RS3	Residual stress by stress double-shot peening
S	Area of semielliptical crack
S_{NDI}	Area of semielliptical crack with $2c = 0.6$ mm and $a = 0.3$ mm
t	Plate thickness
$2w$	Plate width
α_A	Shape correction factor at point A under tensile stress
α_C	Shape correction factor at point C under tensile stress
β_A	Shape correction factor at point A under bending stress
β_C	Shape correction factor at point C under bending stress
ϕ	Angle of crack

cracks by peening are defined as "improving the fatigue limit of peened precracked materials to be 95% or more of fatigue limit of peened smooth materials" (Ref 2-7). ② Despite the existence of pre-cracks that reduce the fatigue limit of nonpeened smooth materials by 40-70%, when the peened materials were fractured with cyclic stresses above the fatigue limit, most of the specimens were fractured from outside the pre-cracks in research by Nakagawa et al.(Ref 3). This peculiar fatigue fracture behavior can be explained using Eq 1 proposed by Ando et al.(Ref 2): ③ In the case of the peened smooth materials, all specimens with $R = -1.0$, 0, and 0.4 were observed to be Stage II nonpropagating cracks (tensile type), as shown in Fig. 6(c). A nonpropagating crack with $R = 0$ can be explained using Eq 1 (Ref 3-8). Furthermore, when observing the residual stress distribution of peened materials in detail, a considerably large local tensile residual stress was observed in research by Yasukawa et al.(Ref 9). Ando et al.(Ref 2) made it possible to qualitatively explain the stage II nonpropagating cracks that occur in the peening material.

Several rotating machines were subjected to cyclic stresses with a stress ratio of $R = -1.0$. These members consist of many designs designed against the fatigue limit, using high-strength materials. Maintenance of these members involves the following problems: (A) During maintenance, because the cracks that should be detected by nondestructive inspection are small, it takes a long time to decrease the reliability. (B) The application of surface crack nondamaging technology by peening is useful for solving problem (A). However, Eq 1, proposed by Ando et al.(Ref 2) to evaluate a_{hml}, has not been proven to be applicable to $R = -1.0$.

Therefore, this paper reports the results of examining the following three characteristics: (i) The adaptability of Eq 1 was verified using the results of $R = -1.0$, as reported in research by Fukuda (Ref 6) and Fukuda et al.(Ref 7). (ii) The aspect ratio (As) dependence of the harmless crack depth (a_{hml}) was analyzed for the three types of residual stress distributions. (iii) Using the results of research by Rummel et al. (Ref 10), Mizutani (Ref 11), and Ochiai et al. (Ref 12), we assumed a crack depth (a_{NDI}) that could be accurately detected by nondestructive inspection. By comparing a_{hml} and a_{NDI} as well

Table 1 Chemical composition of S50C (mass%)

C	Si	Mn	P	S	Cu
0.5	0.2	0.72	0.018	0.018	0.01

as introducing a large and deep compressive residual stress, it was possible to achieve rationalization and improved reliability of maintenance of high-strength steel with a fatigue limit design under a stress ratio of $R = -1.0$.

2. Material, Specimen, and Experimental Method

The material was S50C of HV500 with widths ($2W$) and thicknesses (t) of 10 mm and 3 mm, respectively. Table 1 lists the chemical compositions of the samples. Two types of specimens were used (Fig. 1): smooth and notched. The crack depths (a) with a width of 0.03 mm were 0.04, 0.075, and 0.1 mm (Ref 6, 7). The aspect ratio of the crack ($As = a/c$) was 1.0, where $2c$ is the crack length on the surface. Residual stress was introduced using the cavitation peening (CP) method. The nozzle diameter for jetting high-pressure water was 0.8 mm, and the pressure was 30 MPa. The nozzle diameter for jetting low-pressure water was 20 mm, and the pressure was 0.21 MPa. The distance from the tip of the low-pressure water nozzle to the specimen is 30 mm. The nozzle speed was 3.75 mm/min.

The residual stress was evaluated using x-ray diffractometry (Ref 6, 7). Residual stress was measured by electropolishing the central portion of the surface of the CP-treated specimen, and the distribution in the depth direction was subsequently measured. The measurements were taken using the cos α method with $Cr - K_\alpha$ radiation.

The fatigue test was conducted using a plain bending test with a stress ratio of $R = -1.0$. All tests were performed at a frequency of 20 Hz. The fatigue limit is defined as the maximum stress amplitude at which the specimen can endure 10^7 cycles (Ref 6, 7).

3. Analysis Method

The crack-length dependence of the threshold stress intensity factor range (ΔK_{th}^R) of the fatigue crack propagation proposed by the authors can be evaluated using Eq 1 (Ref 2).

$$\Delta K_{th}^R = 2\Delta\sigma_w^R \sqrt{\frac{l}{\pi}} \cos^{-1}\left[\left\{\frac{\pi}{8l}\left(\frac{\Delta K_{th(l)}^R}{\Delta\sigma_w^R}\right)^2 + 1\right\}^{-1}\right] \quad \text{(Eq 1)}$$

where ΔK_{th}^R and $\Delta K_{th(l)}^R$ are the threshold stress intensity factor ranges of the fatigue crack propagation of the stress ratio R for microcracks and sufficiently large cracks, respectively. $\Delta\sigma_w^R$ is the fatigue limit (range) of the smooth specimen, and when $R < 0$, $\Delta\sigma = \sigma_{max} - \sigma_{min}$, as shown in Fig. 2. l is the half-length of a through crack in an infinite plate.

ΔK^R for the stress ratio $R < 0$ was obtained using the value (σ_{max}) of the tensile stress portion of the cracked specimen in Fig. 2, because the crack closes at $\sigma = 0$. In the
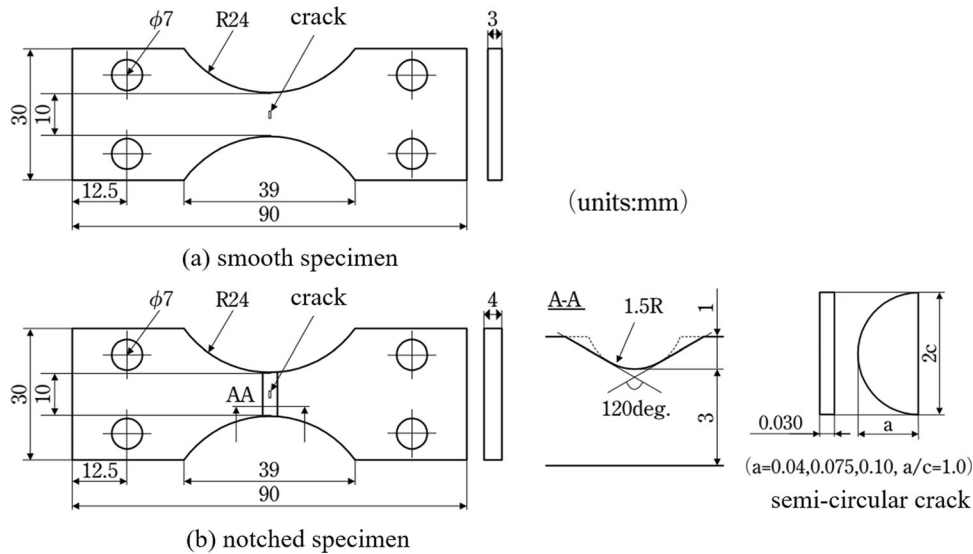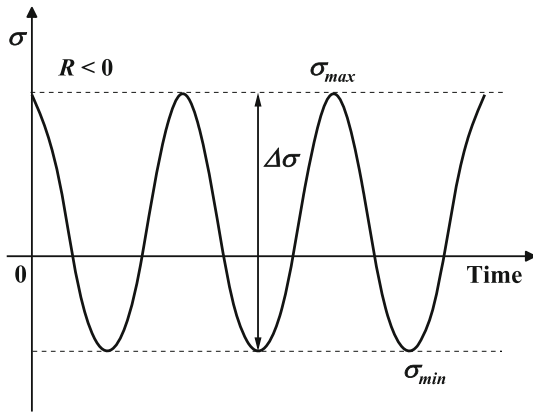
Fig. 1 Shapes of two types of specimens

Fig. 2 Definition of stress in the case of stress ratio $R < 0$ ($\Delta\sigma = \sigma_{\max} - \sigma_{\min}$)

Fig. 3 Schematic illustration of a semi-elliptical crack in a finite plate

case of an infinite plate, it is obtained using Eq 2 and utilizing $\sigma_{\max}$ in Fig. 3.

$$\Delta K^R = \sigma_{\max}\sqrt{\pi l} \tag{Eq 2}$$

When Eq 1 and 2 are applied to a semi-elliptical crack in a finite plate, the equivalent crack length (l_e) is given by Eq 3 and 4 and is substituted in l in Eq 1 and 2.

$$\sqrt{\pi l_e} = \alpha_A \sqrt{\pi a} \tag{Eq 3}$$

$$\sqrt{\pi l_e} = \beta_A \sqrt{\pi a} \tag{Eq 4}$$

where a is the depth of the semi-elliptical crack, and α_A and β_A are the shape correction factors given by the Newman–Raju equation (Ref 14) at the deepest crack part (point A of Fig. 3) when the specimen of the finite plate is subjected to tensile stress or bending stress, respectively. When evaluating l_e corresponding to the outermost surface (point C in Fig. 3), α_A and β_A are substituted by α_C and β_C. ϕ is the angle of crack. Depth (point A) i s 90°, and surface is 0° in Fig. 3.

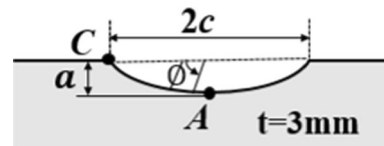The experiments targeted for analysis were performed at a stress ratio of $R = -1.0$. Because the *Non-CP* smooth specimen had a fatigue limit of 528 MPa, a value of 1056 MPa was used for $\Delta\sigma_w^R$ in Eq 1. The effective stress intensity factor range (ΔK_{Tr}) for fatigue crack propagation was evaluated using Eq 5:

$$\Delta K_{Tr} = \Delta K_{ap} + K_r \tag{Eq 5}$$

ΔK_{ap} is the stress intensity factor range, which depends on the bending stress range, because the crack closes at $\sigma = 0$. This was evaluated using the Newman–Raju equation (Ref 14). K_r is the stress intensity factor obtained from the residual stress distribution shown in Fig. 4 based on the *API* method (Ref 15).

4. Results and Discussion

4.1 Residual Stress Distribution

Figure 4 shows the residual stress distribution (RS1) due to cavitation peening (Ref 6, 7). In the case of RS1 (Ref 6, 7), the compressive residual stress at the outermost surface was -725 MPa before the fatigue test and decreased to -581 MPa after the fatigue test. This is because the residual stress was released by fatigue. The maximum depth of the compressive residual stress was $d_o = 0.048$ mm. The residual stress RS1 in Fig. 4 represents the compressive residual stress distribution after the fatigue test.

Table 2 presents the residual stress (σ_O) of the outermost surface and point (d_o) where the residual stress was 0. The compressive residual stresses of RS2 and RS3 are the residual stress distributions assumed to affect on a_{hml}. RS2 and RS3
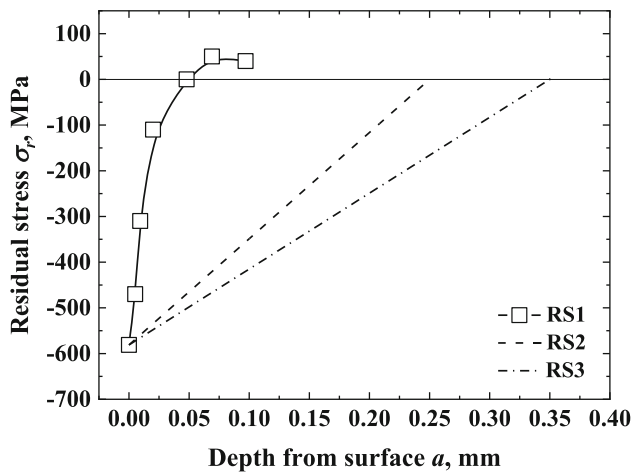
Fig. 4 Compressive residual stress distribution

Table 2 Basic data of residual stress

	σ_0, MPa	d_0, mm
RS1	−581	0.048
RS2	−581	0.25
RS3	−581	0.35

assumed residual stress owing to double-shot peening and stress double-shot peening, respectively (Ref 13). CP has shallow residual stress, and shot peening has different depths depending on the method. RS2 and RS3 were assumed to compare a_{hml} when the surface residual stress is the same, but the depth is different.

4.2 Fatigue Limit

Figure 5 shows the crack-depth dependence of the fatigue limit of *Non-CP* and *CP* specimens (Ref 6, 7). The *Non-CP* smooth specimen has a fatigue limit of 528 MPa, while the CP smooth specimen has a fatigue limit of 699 MPa (Ref 6, 7). The fatigue limit of CP smooth specimen is 33% higher than that of Non-CP smooth specimen. Similarly, the fatigue limit of CP specimens with crack depths of a = 0.04, 0.075, and 0.1 mm increased by 43, 53, and 32%, respectively. This is due to the compressive residual stress introduced into the subsurface by CP.

4.3 Verification of Validity of Equation 1 Using Fatigue Limit by Non-CP and CP Crack Specimens

The validity of Eq 1 was verified using the fatigue limit of the three cracked specimens shown in Fig. 5, fatigue limit (680 MPa, 662 MPa, 680 MPa) of the three nonpropagating cracked specimens shown in Fig. 6, and fatigue limit (449 MPa) of the nonpropagating cracked specimen with a = 0.1 mm. Figure 6 shows three examples of nonpropagating cracks (Ref 6, 7). Figure 6A shows a nonpropagating crack initiated from smooth specimen with a crack of a = 0.04 mm that shows the fatigue limit, and its radius is approximately 0.05 mm. Figure 6B shows a nonpropagating crack initiated from notched specimen with a crack of a = 0.075 mm, which shows the fatigue limit. Figure 6C shows a nonpropagating
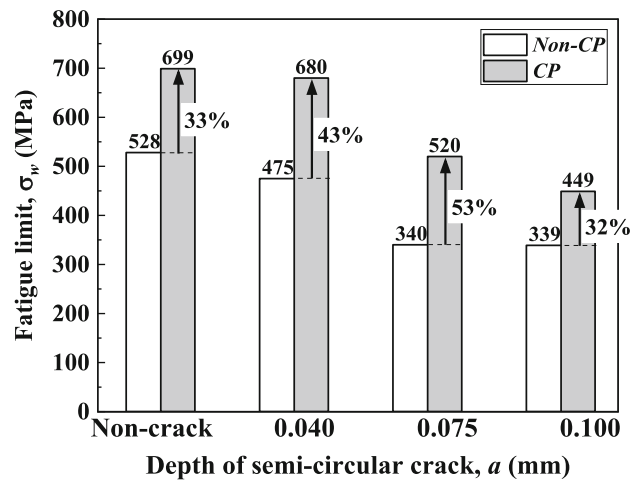

Fig. 5 Fatigue limits of *Non-CP* and *CP* specimens (Ref 6, 7)

crack that was initiated on the back surface of smooth specimen with a crack of a = 0.04 mm showing the fatigue limit. Using σ_{max} of these seven specimens, ΔK_{th}^R was evaluated using the Newman-Raju equation (Ref 14), and $\Delta K_{th(l)}^R$ was evaluated using Eq 1. Consequently, the average value of $\Delta K_{th(l)}^R$ = 5.12 MPa $\sqrt{m}$ was obtained.

Figure 7 shows a comparison of the calculated fatigue limits obtained using this $\Delta K_{th(l)}^R$ with the experimental values. Figure 7 also shows together the results of the non-cavitation peened specimen (Non-CP) of the cracked specimen. In Fig. 7, Δ_w is fatigue limit of nonpeened smooth specimen, and Δ_{wp} is fatigue limit of peened smooth specimen. ' $\pm$ ' in Δ_w and Δ_{wp} means stress amplitude of $R = -1$. The experimental fatigue limit is significantly lower than the calculated value in the case of Non-CP. The crack closes at $\sigma = 0$, but the slit does not close. This was because the evaluated ΔK value for the crack specimen was smaller than its actual value. However, the fatigue limit of the peened crack specimen is slightly higher than the calculated value. In the case of $R \geqq 0$, it can be said that this difference in the fatigue limit does not occur between the cracked specimen and the sharp slit specimen.

Figure 8 shows the relationship between ΔK_{th}^R and crack depth (a) at points A and C, which were obtained by substituting $\Delta\sigma_w^R$ = 1056 MPa in Eq 1. Points A and C are denoted by the solid and dotted lines, respectively. ΔK_{Tr} at points A and C obtained in Eq 5 are indicated by solid and dotted lines, respectively. a_{hml} was calculated as 0.039 mm at point A. Based on the experimental results depicted in Fig. 5, a_{hml} is estimated to be 0.05 mm or slightly larger. Therefore, the calculated value was evaluated as the safe side value. This is because we used $\Delta K_{th(l)}^R$ = 5.12 MPa $\sqrt{m}$, which is the average value obtained from the slit-and-crack specimens. It can be said that Eq 1 is valid not only for $R = 0$ but also for $R = -1.0$.

4.4 Dependence of Residual Stress Distribution and Crack Aspect Ratio (As) of a_{hml} in the Case of R = − 1.0

Figure 9A, B shows the a_{hml} evaluation results for the residual stresses of RS1, RS2, and RS3. Figure 9A, B shows the results of As = 1.0 and 0.7 and of As = 0.4 and 0.1, respectively. Solid lines denote As = 1.0 and 0.4, while dotted lines denote As = 0.7 and 0.1. As can be seen from Fig. 7, a_{hml} is clearly determined at point A. The reason for this is that the
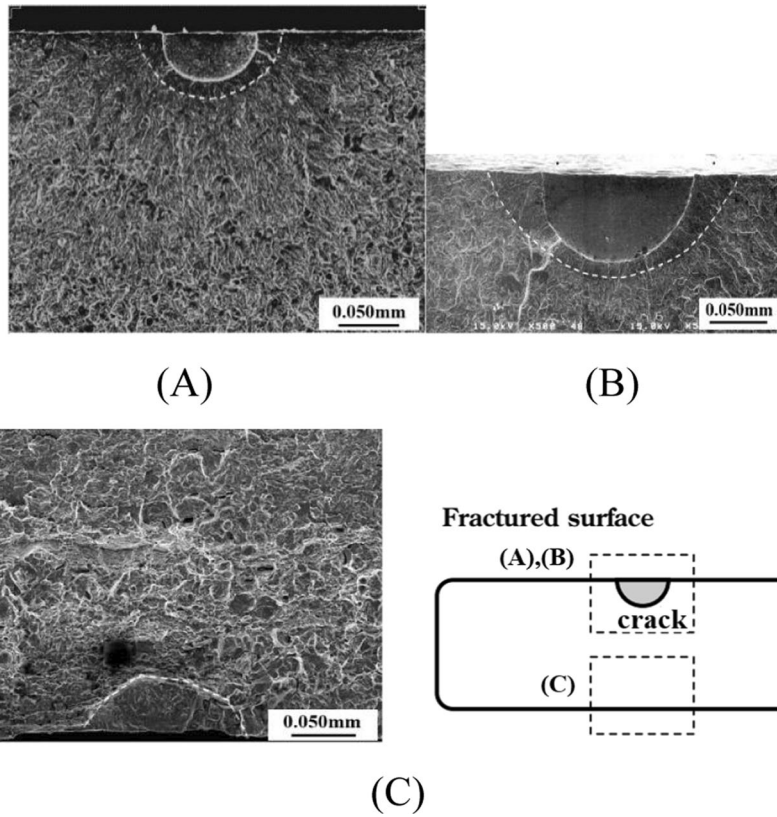
Fig. 6 Harmless crack or nonpropagating crack (Ref 6, 7). (a) Smooth specimen (a = 0.04 mm), (b) notched specimen (a = 0.075 mm), (c) smooth specimen (a = 0.04 mm)
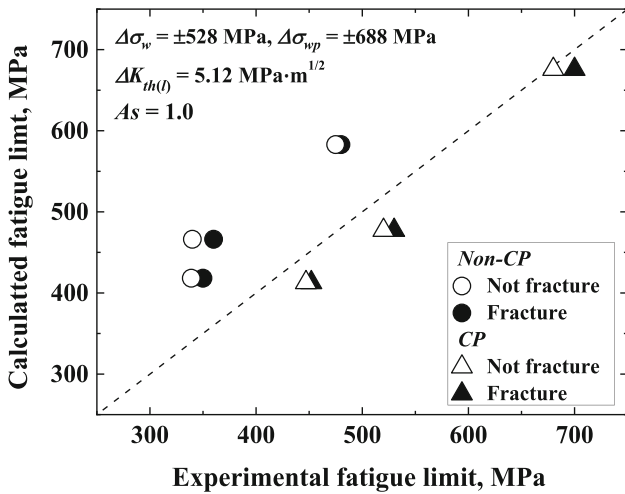

Fig. 7 Comparison of experimental and calculated fatigue limits of the nonpeened and peened crack specimen

Fig. 8 Evaluation of a_{hml} at points A and C in the cases of RS1 and As = 1.0

maximum compressive residual stress always acts at point C on the outermost surface. Therefore, Fig. 9 only shows the a_{hml} evaluation results by point A. a_{hml} is RS1 < RS2 < RS3 for all As, and a_{hml} increases as the compressive residual stress increases, but the influence of As is small. This result is almost the same as that for the case of $R = 0$ in research by Nam et al.(Ref 16).
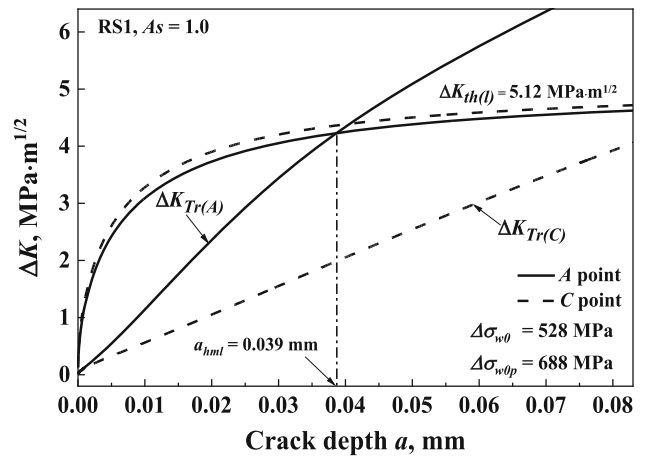
5. Improvement of Integrity and Reliability Against Fatigue Fracture of High-Strength Steel by Combination of Surface Crack Nondamaging Technology and Nondestructive Inspection

5.1 Crack Detection Probability and Nonexistent Crack Depth by Nondestructive Inspection

Rummel et al (Ref 10). In that study, the ultrasonic method was found to be a nondestructive inspection method with the
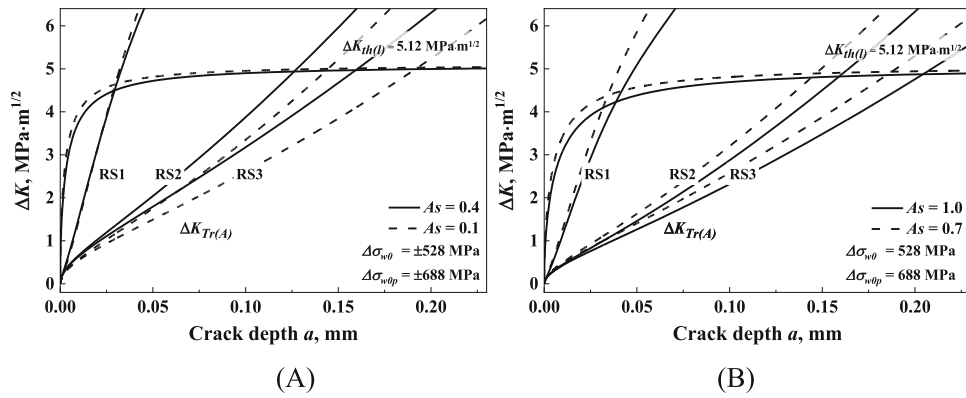
Fig. 9 a- ΔK_{Tr} diagram for determining a_{hml}. (a) As = 1.0 and 0.7, (b) As = 0.4 and 0.1
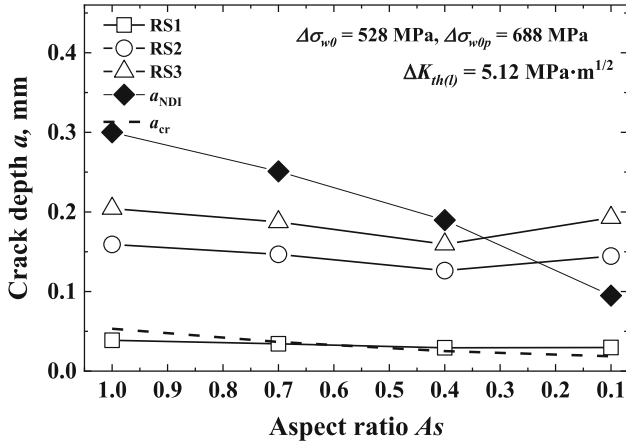
Fig. 10 As dependence of a_{hml}, a_{NDI}, and a_{cr}

highest probability of detecting fatigue cracks. Cracks with a detection probability of 50% had $2c$ = 1.2 mm, a = 0.26 mm (Ref 10, 11). However, since this paper was published in 1974, it can be said to be quite old, and substantial advancements have been made in this field. Although stress corrosion cracking with a depth of 0.4 mm has been successfully measured (Ref 12), the surface length was not recorded. Therefore, the crack was assumed to be semicircular. Considering the above, it is assumed that the very high-performance ultrasonic detection method has sufficient crack detection probability for semielliptical crack of $2c$ = 0.6 mm and a = 0.3 mm. When measuring the echo reflected from the crack front using the ultrasonic detection method, the echo intensity depends on the crack area. The area (S) of a semi-elliptical crack is given by Eq 8.

$$S = \pi ac/2 \tag{Eq 8}$$

In other words, even if As changes, if S of the semi-elliptical crack remains the same, then the crack-detection probability is also the same. Therefore, the S_{NDI} was defined as the area of the semielliptical crack with $2c$ = 0.6 mm and a = 0.3 mm. Equation 9 evaluates the relationship between a_{NDI} given by S_{NDI} and As. The dependence of As is denoted by ◆ in Fig. 10.

$$S_{\text{NDI}} = \pi a_{\text{NDI}}^2/2As \tag{Eq 9}$$

5.2 Safety Assurance of High Tensile Strength Steel ($R = -1.0$) Against Fatigue Limit Design by Application of Surface Crack Nondamaging Technology by Peening

The fatigue limit of *Non-CP* smooth specimen was 528 MPa. If it is designed and applied with a safety factor that is twice the fatigue limit, it can be said that fatigue cracks with a fatigue limit of 264 MPa or less do not exist. Therefore, a_{cr} at which the fatigue limit was 264 MPa was evaluated and is indicated by the dotted line in Fig. 10.

It is believed that members that have been safely used do not have fatigue cracks deeper than a_{cr}. Because a_{NDI} is larger than a_{cr} for all As, it is impossible to detect cracks at depth a_{cr}. Therefore, it is difficult to guarantee the safety of this material through nondestructive inspection alone. However, when the compressive residual stresses due to peening were RS2 and RS3, a_{hml} was considerably larger than a_{cr} for all As. Therefore, in the case of RS2 and RS3, it is possible to guarantee the safety of this member owing to the surface crack nondamaging technology by peening. However, because a_{hml} of RS1 is approximately equal to a_{cr}, it is ultimately difficult to fully guarantee the safety of this member.

6. Conclusions

Ando et al. proposed an evaluation equation for the crack-size dependence of ΔK_{th} for the propagation of microcracks. Because the validity of this equation has not been examined when the stress ratio is negative ($R < 0$), it was evaluated based on previous experimental results. It is known that the surface crack nondamaging technology by peening contributes substantially to the maintenance of stress corrosion cracking as well as the rationalization and high reliability of the maintenance of high-strength steel against fatigue limit design under $R = 0$ stress (Ref 16). Therefore, a_{hml} was evaluated for the previous compressive residual stress (RS1) and the assumed compressive residual stress (RS2, RS3). a_{hml} were compared with a_{NDI} and a_{cr}. The results obtained are as follows:

1. The equation proposed by Ando et al. is also applicable to the case of $R = -1.0$. Moreover, because $\Delta K_{\text{th}(l)}$ is the average value of the slit and cracked specimens, a_{hml} was evaluated as safe.

2. a_{hml} hardly depends on As, but it depends substantially on d_0, and a_{hml} increases as d_0 increases.

3. Compared to a_{cr}, a_{NDI} is considerably larger, which indicates that the safety of this material cannot be guaranteed by nondestructive inspection.

4. In the cases of RS2 and RS3, where the residual stress owing to peening was sufficiently deep, a_{hml} was considerably larger than a_{cr}. Therefore, surface crack nondamaging technology can substantially contribute to the safety assurance of this material.

5. In the case of RS1, which had a shallow residual stress owing to peening, a_{hml} and a_{cr} were almost the same. Therefore, even surface crack nondamaging technologies cannot guarantee the safety of this material.

Acknowledgment

Data Availability

The data that support the findings of this study are openly available in [repository name, e.g., "figshare"] at http://doi.org[-DOI], reference number [reference number].

References

1. P.J.E. Forsyth, Fatigue Damage and Crack Growth in Aluminum Alloys, *Acta Metall.*, 1963, **11**, p 703–715

2. K. Ando, M.H. Kim and K.W. Nam, Analysis on Peculiar Fracture Behaviour of Shot Peened Metal Using New Threshold Stress Intensity Factor Range Equation, *Fatigue Fract. Eng. Mater Struct.*, 2021, **44**, p 306–316

3. M. Nakagawa, K. Takahashi, T. Osada, H. Okada and H. Koike, Improvement in Fatigue Limit by Shot Peening for High-Strength Steel Containing Crack-Like Surface Defect (Influence of Surface Crack Aspect Ratio), *Trans. JSSE.*, 2014, **59**, p 13–18

4. F. Takahasi, Improvement of Fatigue Limit and Acceptable Surface Defect Size for Spring Steel by Shot Peening. Doctor Thesis of Yokohama National Univ. 2008

5. F. Takahashi, A. Tange and K. Ando, Effect of Shot Peening on Fatigue Limit of Surface Flawed Sample, *Fatigue Fract. Eng. Mater. Struct.*, 2008, **31**, p 242–250

6. S. Fukuda, Improvement of Fatigue Limit and Acceptable Surface Defect Size for Automobile Parts by Cavitation Peening. Doctor Thesis of Yokohama National Univ. 2008

7. S. Fukuda, T. Amano, K. Takahashi, K. Matsui, H. Ishigami and K. Ando, Increase in Fatigue Limit and Acceptable Size of Defect for Smooth and Notched Specimen by Cavitation Peening, *Trans. Jpn. Soc. Spring Eng.*, 2009, **54**, p 1–6

8. J. Yasuda, K. Takahashi and H. Okada, Improvement of Fatigue Limit by Shot Peening for High-Strength Steel Containing a Crack-Like Surface Defect: Influence of Stress Ratio, *Int. J. Struct. Integrity*, 2014, **5**, p 45–59

9. S. Yasukawa, S. Ohya, K. Tango, K. Takeda and A. Tange, Microscopic Residual Stress Distribution Measurement on the Surface of Shot Peening, *J. Soc. Mater. Sci. (Jpn).*, 2014, **63**, p 655–661

10. W.D. Rummel, P.H. Todd Jr., S.A. Frecska, and R. A. Rathke, The Detection of Fatigue Cracks by Nondestructive Testing Methods. NASA Contractor Report (NASA-CR-2369). 1974

11. Y. Mizutani, Nondestructive Inspection of Metal Fatigue, *Ind. Mater. (Jpn).*, 2008, **56**, p 86–89

12. M. Ochiai, T. Miura and S. Yamamoto, Lase-Ultrasonic Nondestructive Testing and Its Application to Nuclear Industry, *Toshiba Rev. (Japan).*, 2006, **61**, p 44–47

13. H. Ishigami, K. Matsui, Y. Jin and K. Ando, A Study on Stress, Reflection and Double Shot Peening to Increase Compressive Residual Stress, *Fatigue Fract. Eng. Mater. Struct.*, 2000, **23**, p 959–963

14. J.C. Newman Jr. and I.S. Raju, An Empirical Stress-Intensity Factor Equation for the Surface Crack, *Eng. Fract. Mech.*, 1981, **15**, p 185–192

15. American Petroleum Institute. Recommended Practice 579 (Fitness for service). American Petroleum Institute. 2000:C3-C10

16. K.W. Nam, K. Ando, M.H. Kim and K. Takahashi, Improving Reliability of High Strength Steel Designed Against Fatigue Limit Using Surface Crack Nondamaging Technology by Shot Peening, *Fatigue Fract. Eng. Mater. Struct.*, 2021, **44**, p 1602–1610